ELSEVIER

Journal of Marine Systems 38 (2002) 31–45

JOURNAL OF MARINE SYSTEMS

www.elsevier.com/locate/jmarsys

Uptake of atmospheric carbon dioxide in the Barents Sea

Staffan Kaltin [a,*], Leif G. Anderson [a], Kristina Olsson [b,1], Agneta Fransson [a], Melissa Chierici [c]

[a] *Department of Analytical and Marine Chemistry, Göteborg University, Kemivägen 10, Gothenburg 412 96, Sweden*

[b] *Norwegian College of Fishery Science, University of Tromsø, Tromsø N-9037, Norway*

[c] *Institute of Ocean Sciences, Centre for Ocean Climate Chemistry, P.O. Box 6000, 9860 West Saanich Road, Sidney, British Columbia, Canada V8L 4B2*

Received 6 July 2001; accepted 14 June 2002

Abstract

The uptake of atmospheric carbon dioxide has been estimated from data collected in 1999 along a transect in the Barents Sea ranging from 72.5°N, 31°E to 78.2°N, 34°E. The uptake has been calculated from the change in total dissolved inorganic carbon, total alkalinity, nitrate and salinity in the water column and from the conservation of mass. The average uptake of carbon dioxide in Atlantic water from late winter until the time of investigation (about 3 months) was estimated to be 29 ± 11 g C m^{-2}. The uptake estimate has been compared with integrated air–sea flux calculated from the wind speed and the difference in fCO_2 between the atmosphere and the ocean. The computed air–sea flux has been compared to estimates of new production, with the latter having a clearer trend of decreasing values with increasing latitude than for the air–sea flux. This could be explained by the decreasing surface water temperature with increasing latitude, indicating that cooling (increasing the solubility of CO_2) is an important factor in driving the air–sea flux. This fact might be different if our study had been performed later in the season.

Keywords: Barents Sea; Carbon dioxide; Air–sea exchange; Dissolved inorganic carbon; C/N ratio; Carbon overconsumption

1. Introduction

The deep water formation on the Arctic shelves, especially in the Barents Sea, has recently been emphasised to be of high importance for the global oceanic circulation (Mauritzen, 1996). The cooling of the Atlantic water flowing north through the Barents Sea, together with the brine release during sea ice formation (Midttun, 1989), increases the density of the water, which enables it to penetrate to intermediate and deep layers in the Arctic Ocean (e.g., Schauer et al., 1997; Anderson et al., 1999). Cooling increases the carbon dioxide solubility and hence lowers the fugacity of carbon dioxide (fCO_2) in the ocean surface layers, giving the ocean a potential to take up carbon dioxide from the atmosphere. Primary produc-

* Corresponding author. Tel.: +46-31-772-2288.
E-mail address: kaltin@amc.chalmers.se (S. Kaltin).
[1] Present address: Akvaplan Niva, Polar Environmental Center, Tromsø, Norway.

0924-7963/02/$ - see front matter © 2002 Elsevier Science B.V. All rights reserved.
PII: S0924-7963(02)00168-9

tion further enhances the carbon dioxide air–sea flux as phytoplankton consumes CO_2 during assimilation, and thus lowers fCO_2. The Barents Sea has been shown to be a region with extensive biological production (Walsh, 1989; Sakshaug et al., 1994), though with large spatial variability. Part of the atmospheric carbon dioxide that is taken up in the Barents Sea will be sequestered for long times (>100 years) through the formation of waters that penetrate intermediate and deep waters of the Arctic Ocean (Schlosser et al., 1990).

The climatic conditions in the Barents Sea show large interannual and annual variations, which strongly depend on the amount and properties of the inflowing Atlantic Water (Loeng et al., 1997). Ådlandsvik and Loeng (1991) proposed that the climate of the Barents Sea oscillates between a warm state (low air pressure, high temperature, increased Atlantic inflow and little ice cover) and a cold state with opposite characteristics. A clearly higher primary production has been observed during warm years (Slagstad and Wassmann, 1996). Strong indications have been found for a relationship between the North Atlantic Oscillation (NAO) index and the location of the ice edge (Fang and Wallace, 1994; Vinje, 1997). Also, variations in temperature and salinity of the inflowing Atlantic water have been shown to correlate with NAO index (Furevik, 2001). The variability of the deep water formation in the Barents Sea has been proposed to be associated with the net inflow to the Barents Sea (Häkkinen, 2000).

It has been speculated that possible alterations in the Barents Sea climate caused by a potential future climate change scenario can have a significant effect on the sequestering of atmospheric carbon by the ocean (Anderson and Kaltin, 2001). In order to resolve this issue, we need to better understand the processes that determine the sequestering of atmos-

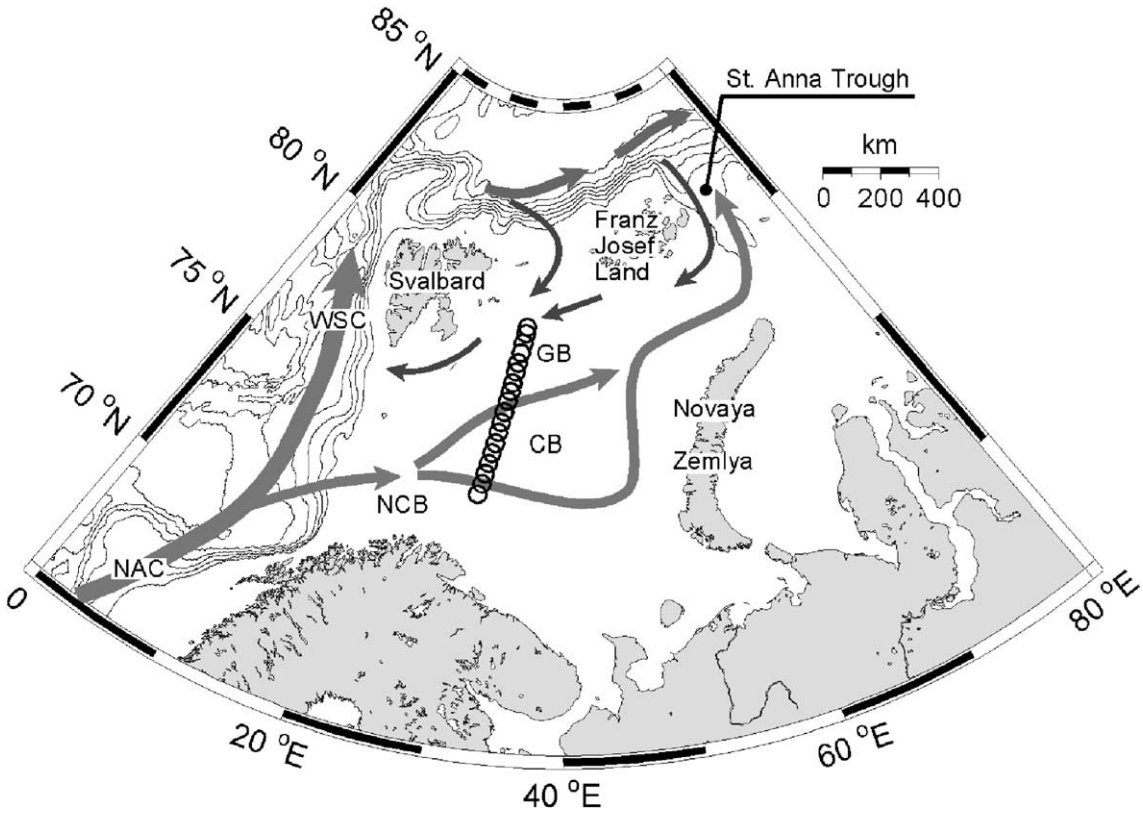

Fig. 1. Map of the Barents Sea showing the predominant currents. The circles represent the station positions. NAC, Norwegian Atlantic Current; WSC, West Spitsbergen Current; NCB, North Cape Bank; CB, Central Bank; GB, Great Bank. The interval between the isobaths is 500 m.

pheric carbon in the Barents Sea, as well as estimates on the magnitude of air–sea CO_2 fluxes.

Fransson et al. (2001) estimated the atmospheric uptake of atmospheric carbon in the Barents Sea to be 44 ± 10 g C m^{-2} (integrated over the upper 150 m) by comparing the relative deficit in inorganic carbon in the North Atlantic water flowing into the Barents Sea via the Bear Island–Northern Norway section and the water flowing out through the St. Anna Trough (Fig. 1). In this study, we estimate the uptake of atmospheric carbon from late winter until early summer in 1999, along a transect across the marginal ice zone (MIZ) in the Barents Sea from 72.5°N, 31°E up to 78.2°N, 34°E (Fig. 1).

2. Physical conditions in the Barents Sea

The northward-flowing Norwegian Atlantic Current follows the Norwegian coast and splits into two branches outside the Barents Sea. One branch enters the Barents Sea via the southwestern boundary (Loeng et al., 1997), while the other continues northwest of Svalbard. In the Barents Sea, the Atlantic water is further divided into two main flow paths at the Central Bank–North Cape Bank sill. One path turns south of the Central Bank while the other flows north of it (Harris et al., 1998). North of Novaya Zemlya, the two paths merge and flow east between Franz Josef Land and Novaya Zemlya, after which it turns north through the St. Anna Trough into the deep Arctic Ocean (e.g., Schauer et al., 1997).

The branch of the Norwegian Atlantic Current that continues to the north turns into the West Spitsbergen Current and partly enters the Arctic Ocean, where it follows the continental margin to the east (Bourke et al., 1988). A small fraction of this water turns south into the Barents Sea, both between Svalbard and Franz Josef Land, and between Franz Josef Land and Novaya Zemlya (Dickson et al., 1970). In the Barents Sea, this water is usually referred to as Arctic water (e.g., Loeng, 1991). Due to its origin and that the main part of this water only has made a short visit in the Arctic Ocean, we here call it cold Atlantic water (see Section 3.3.1). In the Barents Sea, the Atlantic water and the cold Atlantic water are separated by the Polar Front.

Bottom water is formed at various places in the Barents Sea. At the Central Bank and the western Novaya Zemlya shelf, the density of the water is first increased by cooling followed by brine released during sea ice formation, which further increases the density (Midttun, 1985; Loeng, 1991).

3. Methods

3.1. Data

Data are presented from stations located along a south-to-north transect in the Barents Sea, visited during the three ALV (Arktisk Lys og Varme; see Reigstad et al., 2002), cruises March 17–23 (I), May 17–30, 1998 (II) and June 28–July 12, 1999 (III). In this work, we focus on the July 1999 data as they have the best coverage and quality with regards to the carbonate system parameters. The 1998 data are used in the evaluation of the mixed layer depth (MLD) and in the calculations of the air–sea CO_2 based on the difference in fugacity between the atmosphere and sea surface, and wind field. The cruise in March has only been used for evaluating the physical regime, since not enough relevant chemical data are available from that cruise.

Seawater samples were taken at standard depths by means of a rosette sampler equipped with 12 Niskin bottles of 5-l volume. Data from stations along the transect have been divided into latitudinal sections A–E based on the dominating oceanographic regimes in the surface water (Table 1). The most northerly station was located at the edge of the close pack ice. The marginal ice zone was found at section D during the July 1999 cruise. The data used in this work are temperature, salinity, nitrate, phosphate, pH, total dissolved inorganic carbon (C_T) and total alkalinity (A_T). These parameters were all determined during both May 1998 and July 1999, except for C_T that only was determined during July 1999. Salinity and temperature were measured in situ using a Neil Brown MARK III CTD (for more details, see Reigstad et al., 2002).

3.2. Analytical methods

Nitrate was determined using a standard spectrophotometric technique, first reducing nitrate to nitrite and using an azo dye as indicator (e.g., Grasshoff,

Table 1
Station numbers, location of sections A–E during July 1999 (longitudes are between 31°E and 34°E) and surface water characteristics

Section	Latitudes	Station number	Salinity	Temperature (°C)	Nitrate (μM)
A	72.5–74°N	1–5	34–35	> 6	< 1
B	74–75°N	6–8	34–35	~ 4	~ 1
C	75–76°N	9–11	~ 35	~ 4	2–5
D[a]	76–77.1°N	12–15	< 34	0–1	0–4
E	77.1–78.2°N	16–19	~ 34	< −1	> 5

[a] Location of ice edge.

1983). Deviation between duplicate samples was ± 0.15 μM in the range 5–6 μM and ± 0.2 μM at concentrations greater than 11 μM.

During July 1999, total dissolved inorganic carbon was determined by gas extraction of an acidified seawater sample followed by coulometric titration (Johnson et al., 1985, 1987). The analysis was done within hours of sample collection. Total alkalinity was also determined on board the ship by titrating the samples with 0.05 M HCl and measuring the change in pH with a potentiometric method (Haraldsson et al., 1997). The precision for both C_T and A_T was determined by two to four repeated measurements of randomly chosen samples (without any time delay between repetitions). The average standard deviation was 3.7 ± 1.8 μmol kg^{-1} for 19 C_T samples (mean of 2.4 repetitions) and 1.4 ± 0.9 μmol kg^{-1} for 11 A_T samples (mean of 2.5 repetitions). The accuracy was set at each change of cell solution with a certified reference material supplied by A. Dickson (Scripps Institution of Oceanography, USA).

pH was determined spectrophotometrically using *m*-cresol purple as indicator (Clayton and Byrne, 1993; Lee and Millero, 1995), with the measurements performed in a 1-cm flow cell thermostated to 15 °C. The temperature was determined in the seawater sample upstream of the flow cell. The average standard deviation was 0.0006 ± 0.0006 for the 15 samples that were determined in duplicates. The accuracy is set by the accuracy in the temperature measurements and the accuracy in the determination of the stability constant of the dye, being approximately ± 0.002 (Dickson, 1993). The magnitude of the perturbation to seawater pH caused by addition of the indicator solution was calculated and corrected for by the use of the method described by Chierici et al. (1999).

During May 1998, pH was determined potentiometrically at laboratory temperature (13 ± 1 °C) using a Hansson buffer ($S = 35$) to calibrate the electrode pair and Gran evaluation of the equivalence point. Precision was obtained by measurement of randomly selected duplicate samples, and found to be ± 0.01. A_T was determined by the same method as during July 1999, but the samples were analysed in a laboratory on shore. Samples were collected in 250-ml HPDE bottles and 2.5 ml of 2 mM $HgCl_2$ was added as preservative directly after sampling. The samples were stored at 5 °C in a refrigerator until analyses, which took place within 1 year after sampling. To eliminate possible effect of the addition of preservative on speciation, randomly selected samples were spiked with additional $HgCl_2$. The average standard deviation was 0.5 ± 0.5 μmol kg^{-1} for 14 duplicate samples. Also, the accuracy for these A_T samples was determined by analysing the Dickson reference material.

The fugacity of carbon dioxide (fCO_2) was calculated with the CO_2 program developed by Lewis and Wallace (1998) using A_T and pH as input parameters. The total hydrogen ion scale and the carbon dioxide constants from Roy et al. (1993, 1994) were used. The same program was used to compute C_T when not measured (at stations 1–12 in July 1999). A 1% increase in the result of the measured parameter, pH and A_T, gives a percentage change in the calculated C_T, corresponding to 0.8% when including the estimated uncertainty of K_0, K_1 and K_2 (Dickson and Riley, 1977).

3.3. Calculations

In order to compute the change in dissolved inorganic carbon caused by air–sea flux and biological processes, we want to know the concentrations just before the productive season started, hereafter noted preformed concentrations. The mixing of water masses that takes place between winter and the time of

investigation complicates such an assessment. Our approach to solve this is to first identify the source waters, then to determine the concentrations of the constituents relevant for the carbon flux calculations in these, evaluate the fractions of source waters in each sample and, finally, to compute the preformed concentrations from this information.

3.3.1. Source waters

Fig. 2 shows the temperature and salinity properties for the samples collected in July 1999. The seawater source for all samples is Atlantic water, which has undergone modification within the Barents Sea, or nearby. The notations of these source waters are shown in bold in Fig. 2. In addition to the T–S properties, we have restricted the use of data when evaluating the source water concentrations to an upper depth (120 m for Aw and 90 m for cAw) and a northern latitude boundary of 74°N for Aw. This is in order to find the core of the Atlantic and the cold Atlantic waters with properties changed the least since wintertime. We have used lower case letters in our source water abbreviations to stress that this is not a traditional water mass definition.

The property of the low salinity source water (here called freshwater) has been estimated separately for the two regions, north and south of 74°N, as exemplified for total alkalinity in Fig. 3. The A_T concentration in the freshwater is estimated from the

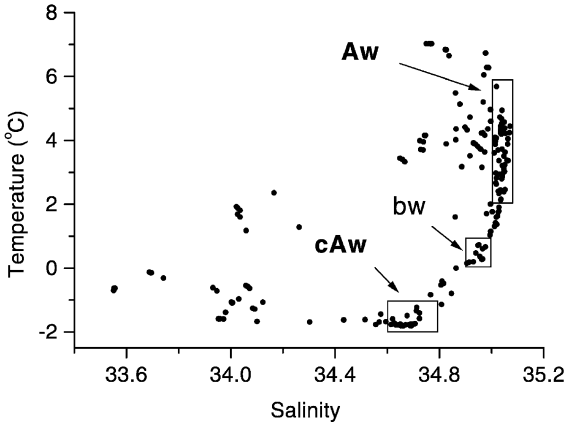

Fig. 2. Temperature–salinity diagrams showing all data from July 1999. Waters having characteristic T–S properties are noted with boxes; Atlantic water (Aw) with S>35 and T>2 °C, and cold Atlantic water (cAw) with T< − 1 °C and 34.6< S<34.8.

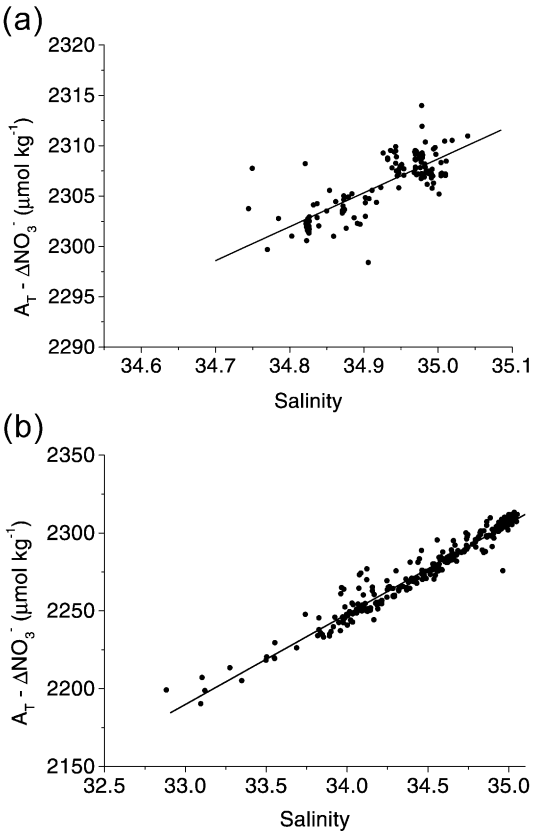

Fig. 3. Nitrate corrected total alkalinity as a function of salinity for samples collected in May 1998 and July 1999, south of 74°N (a) and north of 74°N (b). The linear regressions are equal to $y=33.7x+1130$ ($R^2=0.62$), south of 74°N, and $y=58.1x+273$ ($R^2=0.95$), north of 74°N. Note the different scales in the two diagrams.

intercept with the y-axis in a diagram of A_T versus S, where the measured alkalinity has been compensated for the change in alkalinity caused by consumption of new nitrate during primary production. As the concentration of A_T and C_T are almost equal in fresh water (at least relative to the uncertainty in our estimate), we have used the same concentration (Table 2) for both constituents. Total alkalinity in Arctic rivers is typically above 1000 µmol kg^{-1} (Olsson and Anderson, 1997). Reported concentrations of nitrate in the freshwater, both river runoff and sea ice melt, span a fairly large range (e.g., Gordeev et al., 1996) and we have set the mean concentration to 4 µM. However, our calculations are not sensitive to the choice of freshwater endmember, as the fraction of

Table 2
The source waters concentrations in different waters and areas

Parameter	Aw	cAw	Freshwater	
			<74°N	>74°N
Salinity	35.04	34.70	0	0
C_T (μmol kg^{-1})	2136	2151	1130	273
A_T (μmol kg^{-1})	2309	2288	1130	273
NO_3^- (μM)[a]	11.7	10.2	4	4

[a] To avoid confusion, NO_3^- concentration is given in the same unit as in related papers within this volume (μM). However, all calculations are based on concentrations in micromoles per kilogram.

freshwater is low. North of 74°N, the freshwater fraction has low alkalinity and thus probably originates mainly from melted sea ice with a small contribution of river runoff. For waters south of 74°N, the alkalinity in the freshwater is clearly higher (Fig. 3), indicating contribution from river runoff.

3.3.2. Preformed state and preformed concentrations

For every water sample, a preformed concentration, C^0, is calculated by assuming that the specific water sample consists of a freshwater and a seawater source. The preformed concentration of any constituent in a water sample is defined as:

$$C^0 = X_f C^f + X_s C^s \quad (1)$$

where C^f is the concentration in the freshwater source and C^s the concentration in the seawater source. X_f is the fraction of freshwater and X_s is the fraction of seawater in a water sample. The freshwater fraction is calculated by:

$$X_f = \frac{S^s - S^{meas}}{S^s} \quad (2)$$

where S^{meas} is the measured salinity (equal to S^0 as salinity is conservative after the preformed water has been formed). The seawater fraction, X_s, is equal to $1 - X_f$.

A preformed concentration here represents the concentration a water sample had at a point of time before the time of investigation, *a preformed state*. The preformed concentration, which is determined by which fresh and sea source waters are used, thus determines the point of time the preformed state represents. The choice of source waters for the computations in the different sections is given in Table 3.

3.3.3. Change in carbon concentrations

The shift in the inorganic carbon concentration in the ocean due to exchange with the atmosphere ($\Delta C_T^{air-sea}$) from the time of the *preformed state* until the time of investigation can be computed by Eq. (3):

$$\Delta C_T^{air-sea} = \Delta C_T^{bio} - \Delta C_T. \quad (3)$$

The change in the total inorganic carbon concentration in the water column, ΔC_T, is the difference between the preformed and the measured concentrations ($C_T^0 - C_T^{meas}$). The change caused by biological new production, ΔC_T^{bio}, is computed according to Eq. (4):

$$\Delta C_T^{bio} = C/N\,\Delta NO_3^- + 0.5(\Delta A_T + \Delta NO_3^-). \quad (4)$$

C/N represents the carbon-to-nitrogen ratio during fixation of organic matter. ΔNO_3^- is the change in nitrate concentration and ΔA_T is the change in total alkalinity, both computed as the difference between the preformed and the measured concentrations. In Eq. (4), the change caused by production of organic soft matter equals $C/N\,\Delta NO_3^-$ and the change caused by production of hard parts (mainly $CaCO_3$) equals 0.5 ($\Delta A_T + \Delta NO_3^-$).

Several recent studies of the relationships between carbon and nitrogen consumption during biological production (e.g., Sambrotto et al., 1993; Banse, 1994; Körtzinger et al., 2001) have reported substantially higher carbon consumption relative to nitrogen than the traditional C/N ratio of ~6.6 (Redfield et al., 1963). We have used a C/N ratio, determined by

Table 3
Source waters used for the calculations in the different sections

Section	Seawater source	Freshwater source
A	Aw	<74°N
B	Aw	>74°N
C	Aw	>74°N
D	Aw/cAw[a]	>74°N
E	cAw	>74°N

[a] A mixture of 1:1 of these waters was used.

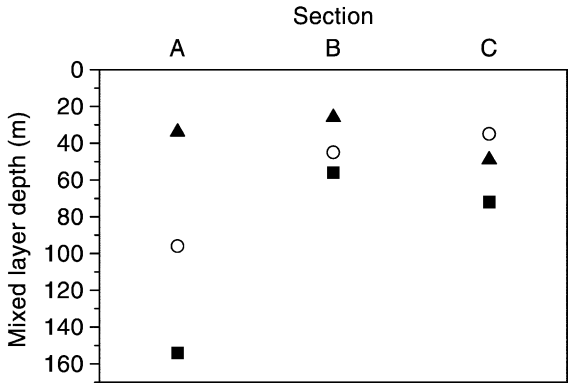

Fig. 4. Mixed layer depth (MLD) in March 1998 (■), May 1998 (○) and July 1999 (▲) at sections A–C.

Takahashi et al. (1985), equal to 8.75 and compared the results with those of the traditional C/N ratio.

3.3.4. Mixed layer depth

In order to compute the depth-integrated change caused by air–sea exchange as well as biological activity, the mixed layer depth (MLD) is needed. The MLD was determined according to Glover and Brewer (1988) as the depth of density that is calculated with the surface salinity and a temperature 0.5° lower than the measured surface temperature. The average MLD values computed for sections A–C in March 1998, May 1998 and July 1999 are shown in Fig. 4.

4. Results and discussion

4.1. New production and air–sea CO_2 flux from change in relevant constituents

The main objective of this study is to evaluate the oceanic uptake of atmospheric CO_2 in the Barents Sea. In order to do this, we need both a time and a vertical resolution perspective. The time for the estimated uptake is determined by the time when the preformed state was set, which is the preceding winter, and the estimates thus represent the time from winter to the time of investigation. Fig. 5 shows the ΔC_T^{bio} and ΔC_T versus depth at the different sections in July 1999. According to Eq. (3), a situation with $\Delta C_T^{bio} > \Delta C_T$ represents net uptake of CO_2 from the atmosphere and $\Delta C_T^{bio} < \Delta C_T$ represents net outgassing. Integrating the ΔC_T^{bio} and the $\Delta C_T^{air-sea}$ ($= \Delta C_T^{bio} - \Delta C_T$) profiles gives the new production and net uptake of atmospheric carbon, as summarised in Tables 4 and 5. The discussion of the results is based on a C/N ratio equal to 8.75 (Table 4).

The computed new production in sections A–C is in the range of 43–76 g C m^{-2} (Table 4). The variation in the range is about the same as the variation in annual primary production (40–90 g C m^{-2}) for the whole Barents Sea, when comparing a cold and a warm year (Slagstad and Wassmann, 1996). Wassmann et al. (1999) estimated the new production in the central Barents Sea until late May in 1993 to be 27 ± 28% g C m^{-2}. Based on the same nutrient data set we have used, Reigstad et al. (2002) estimated the average new production for the entire water column along the transect to be 54 g C m^{-2}. These three other estimates are based on a C/N ratio equal to 6.6.

Uptake of CO_2 in the Atlantic water (sections A–C) is two to four times higher than in the cold Atlantic water (section E) in July 1999. This result is not surprising since the cold Atlantic water is ice-covered during most time of the year, while the Atlantic water mostly is open. Hence, the length of the season is a main factor for both new production and air–sea flux. For the new production, there is a clearer trend of decreasing values with increasing latitude than for the air–sea flux. This could be explained by the decreasing surface water temperature with increasing latitude, indicating that cooling (increasing the solubility of CO_2) is an important factor in driving the air–sea flux. This fact might be different if our study had been performed later in the season.

4.2. Vertical resolution in depth-integrated assessments

Sections A–C showed a decrease in MLD from March to July except for section C, where the MLD in July 1999 was slightly shallower than in May 1998 (Fig. 4). This exception can easily represent annual variability. The average MLD was greatest in section A, ranging from ~150 m in March 1998 down to only ~30 m in July 1999. The MLD did not vary much in sections B and C with an average around 50 m. MLD for sections D and E was not calculated with

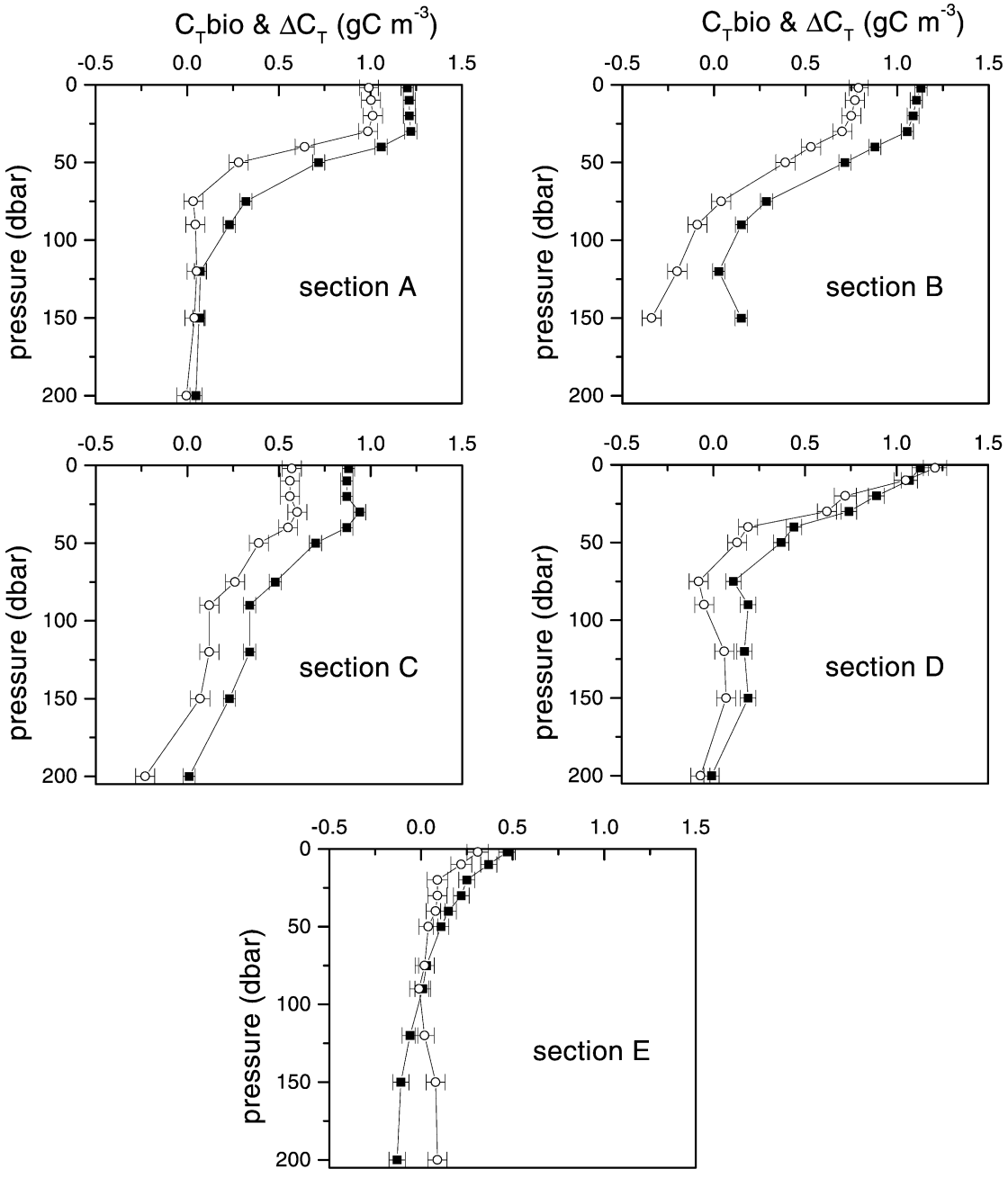

Fig. 5. New production, ΔC_T^{bio} (■), and the observed change in dissolved inorganic carbon, ΔC_T (○), versus depth at the different sections during July 1999. The error bars represent the uncertainties due to analytical imprecision, variability in preformed concentrations and the uncertainty in the freshwater estimate (see Section 4.4).

Table 4
New production (NP) and uptake of carbon dioxide from the atmosphere ($U^{air-sea}$) calculated with C/N = 8.75 and integrated over the upper 50 and 100 m of the water column (Fig. 5)

Section	NP, g C m^{-2}		$U^{air-sea}$, g C m^{-2}	
	July 1999		July 1999	
	50 m	100 m	50 m	100 m
A	57 ± 2	76 ± 3	14 ± 3	28 ± 6
B	50 ± 2	68 ± 3	17 ± 3	30 ± 6
C	43 ± 2	68 ± 3	16 ± 3	28 ± 6
D	39 ± 2	49 ± 4	6 ± 3	17 ± 7
E	13 ± 2	15 ± 4	6 ± 3	8 ± 7
A–C average	50 ± 3	70 ± 6	16 ± 5	29 ± 11
A–E average	40 ± 4	55 ± 8	12 ± 7	22 ± 14

The error estimates include the analytical error, the variability in the source water concentration and the uncertainty in the freshwater estimate (see Section 4.4).

the described method (see Section 3.3.4), but the density profiles (not shown) of these sections clearly reveal that the mixed layer was less than 50 m. The nitrate concentration in March 1998 was very homogenous from the surface down to 200 m depth (average: 11 ± 0.3 μM), indicating that the water column is well mixed during winter. The spring bloom has not yet started at the time of this investigation (Reigstad et al., 2002).

The calculated mixed layer depth gives us an indication of which depth integration is the most representative for the uptake of atmospheric CO_2 since the winter. Still these will be rough estimates, as the evolution of the MLD is not known. For instance, storms are likely to disrupt and deepen the mixed layer for shorter time periods during the productive season. Sakshaug et al. (1995) found a strong connection between sudden increases in mixed layer depth and strong winds during recurrent atmospheric low pressures in the Barents Sea.

According to the calculated MLD (Fig. 4), the computed uptake of atmospheric carbon in the upper 100 m would be a better estimate for section A, while the uptake in the upper 50 m would be a better estimate for sections B–C (Table 4). The new production signature is observed all the way down to 150 m ($\Delta C_T^{bio}>0$) in section C (Fig. 5). This indicates mixing down to 150 m depth during the productive season. As this depth by far exceeds the calculated MLD for section C during all cruises (Fig. 4), the MLD for this section has probably been greater than the computed depth at some time during the productive season. Integrating the air–sea uptake down to 50 m for this section, as proposed above, is hence not deep enough to represent the uptake of CO_2 since the start of the productive season. New production at depths greater than the calculated MLD was also observed in section B, but not to such great depths as in C. The negative ΔC_T at greater depths, where $\Delta C_T^{bio} \approx 0$, is interpreted as carbon taken up from the atmosphere before the start of the productive season. These results can partly be explained by the occurrence of a locally produced bottom water mass found at the Central Bank and the Grand Bank, which likely has taken up atmospheric CO_2 when the water was cooled during winter. The cold bottom water, bw, is noted in the T–S diagram (Fig. 2) and is the densest water found along the transect.

Water below 100 m in section E is greatly influenced by bottom water with lower nitrate and higher C_T concentrations than the cold Atlantic water, which was used as source water for the calculation at this section. Thus, the ΔC_T^{bio} and ΔC_T profiles at depths greater than 100 m are not appropriate for this discussion.

4.3. Air–sea CO_2 fluxes from wind field and ΔfCO_2 data

The computed uptake of atmospheric CO_2 in Table 4 can be compared to directly calculated fluxes to the ocean from the wind speed and the difference in fCO_2

Table 5
New production (NP) and uptake of carbon dioxide from the atmosphere ($U^{air-sea}$) calculated with C/N = 6.6 and integrated over the upper 50 and 100 m of the water column (Fig. 5)

Section	NP, g C m^{-2}		$U^{air-sea}$, g C m^{-2}	
	July 1999		July 1999	
	50 m	100 m	50 m	100 m
A	43 ± 1	57 ± 3	0 ± 3	9 ± 6
B	38 ± 1	50 ± 3	4 ± 3	13 ± 6
C	33 ± 1	51 ± 3	5 ± 3	11 ± 6
D	29 ± 1	37 ± 3	−3 ± 3	5 ± 6
E	9 ± 2	11 ± 4	3 ± 3	4 ± 6
A–C average	38 ± 2	53 ± 5	3 ± 5	11 ± 10
A–E average	30 ± 3	41 ± 6	2 ± 7	8 ± 13

The error estimates include the analytical error, the variability in the source water concentration and the uncertainty in the freshwater estimate (see Section 4.4).

between the atmosphere and the ocean, according to Wanninkhof (1992):

$$F^{\text{air}-\text{sea}} = 0.31u^2K_0\sqrt{\frac{660}{Sc}}\Delta f\text{CO}_2. \quad (5)$$

$F^{\text{air}-\text{sea}}$ is the flux of CO_2 across the air–sea interface, K_0 is the solubility of CO_2, u is the wind speed, Sc is the Schmidt number and $\Delta f\text{CO}_2$ is the difference in fugacity between the atmosphere and that of the very surface water.

The uptake of atmospheric CO_2 given in Table 4 is based on the computed preformed concentrations, which in turn are computed from the concentrations in Table 2. As the latter are thought to represent winter values, the uptake in Table 4 is integrated from the winter to the time of investigation. To investigate if it is reasonable to assume that the applied source water concentrations represent the winter concentrations before the productive season started, we make a complementary computation of the air–sea CO_2 flux using Eq. (5). For this, it is necessary to know the wind speed as well as the $f\text{CO}_2$ development over the same time period (from winter until the time of investigation). It is possible to obtain the wind field but not the $f\text{CO}_2$ development; however, a rough estimate can be achieved using the observed $f\text{CO}_2$. This was done by interpolating the $f\text{CO}_2$—calculated from temperature, salinity and the carbonate system parameters in the surface water at the time of the cruises—between the dates of investigation (168 μatm on May 19 and 229 μatm on June 30). As no winter data were available from the March cruise, we used $f\text{CO}_2$ calculated to be 352 μatm from measured A_T and C_T concentrations collected during a cruise in February–March 1994 at position 74.5°N and 16°E. The development of the atmospheric $f\text{CO}_2$ from March to July (from 369 to 365 ppm) at the Ny-Ålesund station on Svalbard (Holmen, 2001) was used for the seasonal progression. No $f\text{CO}_2$ data were available for 1999 but the annual increase during the last decade has been relatively constant (~ 1 ppm). Hence, we set the atmospheric $f\text{CO}_2$ for 1999 equal to the $f\text{CO}_2$ during 1998 plus 1 ppm. This estimate is within the uncertainty of our calculations. A computation using a constant $f\text{CO}_2$ in the water equal to the observed surface water $f\text{CO}_2$ during the cruises was also made.

The interpolated daily wind speeds (average of four measurements per day) during 1999 were used to calculate the daily uptake of CO_2 from wintertime

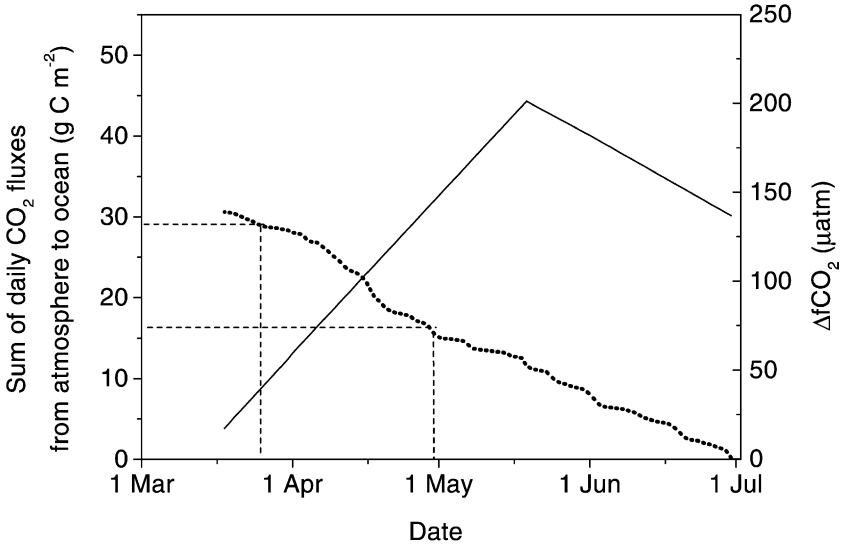

Fig. 6. The sum of the daily fluxes (bold dotted line) from the time of investigation (July 1) and back in time. The daily fluxes were calculated by Eq. (5), the synoptic wind field and $\Delta f\text{CO}_2$ (atmospheric pressure–surface water pressure), shown as a solid line. The horizontal dashed lines represent the calculated average uptake of CO_2 from the atmosphere, $U^{\text{air}-\text{sea}}$ (Table 5), in the upper 50 m (16 g C m^{-2}) and upper 100 m (29 g C m^{-2}) in sections A–C in July 1999. Vertical dashed lines mark the estimated time of the preformed state.

until the time of investigation. Wind speed was taken from the Norwegian Meteorological Institutes hindcast data archive (Eide et al., 1985) and data corresponding to the latitude and longitude range in the different sections along the transect were used. The computations do not consider the ice cover and have thus only been made for sections A–C. The daily uptakes are summarised from July 1 (the time of investigation) and back in time (Fig. 6).

The integrated flux of CO_2, $F^{air-sea}$, shows that about 2 months are needed to take up the amount CO_2 computed for the top 50 m ($U^{air-sea}=16$ g C m^{-2}; Table 4). It takes about 1 month longer to take up the amount of carbon computed for the top 100 m ($U^{air-sea}=29$ g C m^{-2}; Table 4). Both of these estimates are for the linear interpolated ΔfCO_2 data (Fig. 6). If the calculation is done with a constant surface water fCO_2 of 229 μatm, it would take ~ 10 days longer for the upper 50 m and ~ 10 days less for the upper 100 m.

Wind field and ΔfCO_2 drive the uptake from the atmosphere (Eq. (5)). Cooling of surface water increases the solubility and thus lowers the fCO_2, as does primary production. Considering that the spring bloom typically starts in April in this region (Skjoldal et al., 1987; Slagstad and Wassmann, 1996; Wassmann et al., 1999), the time that is needed (Fig. 6) for the uptake presented in Table 4 is reasonable considering the choice of source water used.

4.4. Uncertainties

The most straightforward uncertainties to evaluate are those that arise from analytical imprecision, variability in the preformed concentrations and the uncertainty in the freshwater estimate. The errors noted in Tables 4 and 5 are the square root of the sum of the squares of all individual uncertainties in A_T, C_T and NO_3. Other uncertainties are more difficult to quantify and are discussed below.

4.4.1. C/N ratio

Fig. 7 shows the uptake of atmospheric carbon versus depth at the different sections. In sections A and D, the profiles show a significant decline towards the surface in the uptake or even outgassing of CO_2 in the surface layers. Considering that all sections had an average fCO_2 in the upper 30 m of the water column

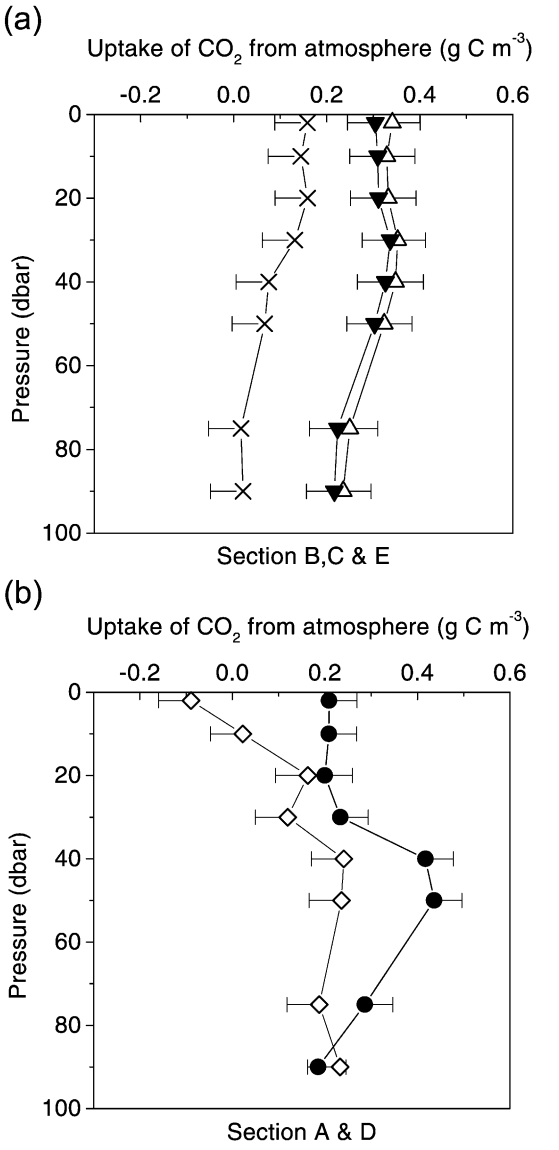

Fig. 7. (a,b) Net uptake of atmospheric CO_2 versus depth at sections A (●), B (△), C (▼), D (◇) and E (×) in July 1999. The error bars represent the uncertainties due to analytical imprecision, variability in preformed concentrations and the uncertainty in the freshwater estimate (see Section 4.4).

between 150 and 250 μatm (significantly lower than the atmospheric partial pressure) and thus acted as sinks at the time of investigation, this does not seem realistic. The results from section D are believed to have greater uncertainties than the others as these sections include the marginal ice zone where there are

great local variations in primary production and the chemical/physical parameters of the water. Section D is also the area where the cold Atlantic and the Atlantic water meet, and here is thus a greater uncertainty in source water concentrations. Still these features alone are not able to explain the shape of these two profiles.

Another possible explanation to those results is that other sources of new nitrogen than nitrate are available for primary production, or alternatively a different C/N ratio during production of organic matter. Overconsumption of carbon relative to nitrogen (higher than the traditional C/N ratio of ~ 6.6) during biological production has, as mentioned, been reported by several authors (e.g., Sambrotto et al., 1993; Banse, 1994; Körtzinger et al., 2001). Bury et al. (2001) calculated a 20% higher production of organic carbon during a 3-week study using measured *f* ratios (the ratio of nitrate uptake to total nitrogen uptake over a long time scale) than when using the traditional Redfield ratio. They also calculated the weighted mean molar C/N uptake ratio to be 8.1 during the same period in the North Atlantic in May. The highest ratios, between 14 and 17, were observed at the end of this period when nitrate was limiting. Michaels et al. (1994) observed in a subtropical North Atlantic study that dissolved inorganic carbon proceeded to decline in the euphotic zone long after nitrate was depleted. In our study, the surface nitrate concentration was lower than 1 μM in the sections with lower calculated uptake or outgassing in the surface layers (A and D) but not other sections. At stations within sections A and D in July 1999, the total uptake rate of dissolved inorganic nitrogen was substantially higher than at stations in other sections (Allen et al., 2002). This could indicate that phytoplankton here was in need for nitrogen after having consumed substantially more carbon relative to nitrogen than the traditional Redfield ratio. We can only speculate that the calculated lower uptake of CO_2 in the surface at these sections is a consequence of this observed phenomenon called 'carbon over consumption' (Toggweiler, 1993). If the C/N ratio that is used in our carbon flux calculations (8.75) is lowered, the relative difference between the uptake of CO_2 in the surface layers and deeper water of these sections increases.

If phytoplankton is consuming recycled nitrate or dissolved organic nitrogen (DON) while consuming "new" inorganic carbon, due to a slower carbon recycling relative to nitrogen, more carbon relative to nitrogen than the C/N ratio in organic matter may be consumed during productive season. As carbon recycling catches up after the productive season, the resulting higher relative increase in C_T/NO_3^- in the water will compensate for this mismatch. Calculating $\Delta C_T^{air-sea} = \Delta C_T^{bio} - \Delta C_T$ at this point of time would mean that ΔC_T has decreased more relative to ΔC_T^{bio} and the higher C/N ratio would not be representative. Dauchez et al. (1996) suggest that at least 6 months are needed to return to a steady state if the C/N ratio in organic matter is to be used to obtain new production from nitrogen converted to carbon. The productive season started significantly less than 6 months before our investigation in July 1999. Combining this with the mentioned reports on carbon overconsumption, it seems reasonable to use a ratio higher than the traditional Redfield ratio for our calculations. If the integrated $F^{air-sea}$ is compared with $U^{air-sea}$ as done in Fig. 6 but with a C/N ratio equal to 6.6 (Table 5), the estimated time for the uptake of CO_2 would be around 10 days in the upper 50 m, and 4 weeks in the upper 100 m. This is unrealistic considering the choice of source waters that was used for the calculations, and thus further stresses the need for a C/N ratio higher than the traditional Redfield ratio. One matter conflicts with our arguments for a higher ratio: heterotrophic bacterial production was found to represent 16–40% of total NO_3^- uptake during July 1999 (Allen et al., 2002) and estimates of C/N ratio in bacteria found in literature often lie within 4–6.5 (Allen, personal communication).

The C/N uptake ratio that is appropriate to use depends on how long a time has passed since production started. Our results may therefore include an error since we have used the same ratio for all sections (A–E). The influence on the calculated average total uptake of atmospheric carbon along the transect due to use of a constant ratio in the calculations is likely significantly less than the effect due to the uncertainty in the average C/N ratio. With today's knowledge, the magnitude of this uncertainty can only be speculated.

4.4.2. Vertical mixing

Our approach to estimate the new production does not consider the vertical mixing of nutrients from under the photic layer. To estimate this uncertainty,

we computed the vertical flux of nitrate, F, according to Law et al. (2001):

$$F = -K_z * \frac{\partial NO_3^-}{\partial z} \quad (6)$$

and

$$N = \sqrt{(g/p_w) * (dp/dz)}. \quad (7)$$

Here K_z is the diffusivity and $\frac{\partial_3^-}{\partial z}$ is the NO_3^- gradient, N is the buoyancy frequency, g is the acceleration due to gravity, p_w is the density and dp/dz is the density gradient. K_z is derived from the buoyancy frequency according to Law et al. (2001).

Taking the average property distribution in sections A–C in July 1999 gave a nitrate flux into the surface mixed layer of 0.1 ± 0.05 μM day^{-1}. This flux gives an underestimate of the new production of about 25% when applied during 1 month. As the nutrient gradient develops over the productive season, this is an absolute maximum number.

As a vertical flux of nitrate also means a flux of carbon, the uncertainty in the air–sea flux due to such mixing is less severe. It is the difference between the ratio of the vertical C_T and nitrate flux and the C/N ratio used in our calculations that determines the uncertainty. The calculated average C_T/NO_3^- vertical flux ratio in July 1999 was 9.5 ± 3. With this difference in ratio taken into consideration, the error in the air–sea flux caused by vertical mixing is $6 \pm 3\%$.

4.4.3. Other uncertainties

To our knowledge, no evidence of nitrogen fixation in polar areas has been reported. If nitrogen fixation occurs in the ocean, the slope of a line with nitrate versus phosphate would be lower than the classical 16. This was not observed during our study, where the slope of the line fitted to the nitrate/phosphate data was 16.

5. Summary and conclusions

Although there are significant uncertainties in our estimate of the air–sea flux of CO_2, it has the advantage over other estimates as it integrates the signal over a time period. Methods based on the measured difference in fCO_2 between the atmosphere and sea surface are fairly accurate in the momentous flux, but require continuous measurements in a specific water mass in order to evaluate the flux over time.

Our estimate of the uptake of atmospheric carbon dioxide in Atlantic water in the upper 100 m in 1999 was 29 ± 11 g C m^{-2}. The estimated time for this uptake was ~ 3 months. This estimate is about two thirds the uptake of 44 ± 10 g C m^{-2} estimated by Fransson et al. (2001) during the residence time of the water in the Barents Sea, which is in the order of 1 year. Our estimate is made under the productive season when uptake of atmospheric carbon probably is greatest. A significant difference between the cold Atlantic (section E) and the Atlantic water (section A–C), with a clearly higher uptake of CO_2 in the latter, was discovered. This result seems reasonable, as the cold Atlantic water is ice-covered during most of the year, while the Atlantic water is mostly open.

The cold Atlantic water in the Barents Sea has been transported a greater distance and also lost more heat than the Atlantic water since these waters were separated west of the southwestern boundary of the Barents Sea. Taking this into account, the cAw would most likely have taken up more CO_2 from the atmosphere than the Aw after they split. The salinity of those waters has also changed since this separation. If the dissolved inorganic carbon concentration in the cAw is corrected to a salinity equal to that in the Aw, assuming that the freshwater fraction in the cAw originates from a water with concentrations equal to the freshwater estimate of water >74°N (Table 2) gives a C_T that is 33 μmol kg^{-1} higher than in the Aw. This implies that the cAw has taken up more carbon than the Aw after they split southwest of the Barents Sea. A significant part of this CO_2 was likely taken up outside the Barents Sea.

To reach a better accuracy in carbon flux calculations based on the relative consumption of nitrate and carbon, the most important issue to examine is the dynamics of the carbon-to-nitrogen consumption ratio. If the average C/N consumption ratio is higher than the C/N ratio in organic matter (Redfield ratio), the importance of primary production will be increased compared to cooling as a driver of air–sea CO_2 flux. Our results indicate that cooling was relatively more important than primary produc-

tion during the time from late winter to early summer in 1999.

Acknowledgements

We are grateful to Paul Wassmann and his group for letting us participate in the ALV experiment and sharing the hydrographic data. The Swedish Research Council supported this research.

References

Ådlandsvik, B., Loeng, H., 1991. A study of the climatic system in the Barents Sea. Polar Res. 10 (1), 45–49.

Allen, A.E., Howard-Jones, M.H., Booth, M.G., Frischer, M.E., Verity, P.G., Bronk, D.A., Sanderson, M.P., 2002. Importance of heterotrophic bacterial assimilation of ammonium and nitrate in the Barents Sea during summer. J. Mar. Syst., this issue.

Anderson, L.G., Kaltin, S., 2001. Carbon fluxes in the Arctic Ocean—potential impact by climate change. Polar Res. 20 (2), 225–232.

Anderson, L.G., Jones, E.P., Rudels, R., 1999. Ventilation of the Arctic Ocean estimated by a plume entrainment model constrained by CFCs. J. Geophys. Res. 104, 13423–13429.

Banse, K., 1994. Uptake of inorganic carbon and nitrate by marine phytoplankton and the Redfield ratio. Glob. Biogeochem. Cycles 8, 81–84.

Bourke, R.H., Weigel, A.M., Paquette, R.G., 1988. The westward turning branch of the West Spitsbergen Current. J. Geophys. Res. 93, 14065–14077.

Bury, S., Boyd, P.W., Preston, T., Savidge, G., Owens, N.J.P., 2001. Size-fractionated primary production and nitrogen uptake during a North Atlantic phytoplankton bloom: implications for carbon export estimates. Deep-Sea Res., Part 1 48, 689–720.

Chierici, M., Fransson, A., Anderson, L.G., 1999. Influence of *m*-cresol purple indicator additions on the pH of seawater samples: correction factors evaluated from a chemical speciation model. Mar. Chem. 65, 281–290.

Clayton, T.D., Byrne, R.H., 1993. Spectrophotometric seawater pH measurements: total hydrogen ion concentration scale calibration of *m*-cresol purple and at-sea results. Deep-Sea Res., Part 1 40, 2115–2129.

Dauchez, S., Legendre, L., Fortier, L., Levasseur, M., 1996. New production and production of large phytoplankton (>5 μm) on the Scotian Shelf (NW Atlantic). Mar. Ecol. Prog. Ser. 135, 215–222.

Dickson, A.G., 1993. The measurement of sea water pH. Mar. Chem. 44, 131–142.

Dickson, A.G., Riley, J.P., 1977. The effect of analytical error on the evaluation of the components of the aquatic carbon-dioxide system. Mar. Chem. 6, 77–85.

Dickson, R.R., Midttun, L., Mukhin, A.I., 1970. The hydrographic conditions in the Barents Sea in August–September 1965–1968. Int. Conf. Explor. Sea. Coop. Res. Rep., Ser. A 18, 3–24.

Eide, L.I., Reiestad, M., Guddal, J., 1985. Database av beregnede vind og bølgeparametre for Nordsjøen, Norskehavet og Barentshavet, hver 6. time for årene 1955–81. The Norwegian Meteorological Institute, Oslo, 38 pp.

Fang, Z., Wallace, J.M., 1994. Arctic sea ice variability on a time scale of weeks and its relation to atmospheric forcing. J. Climate 6, 1897–1914.

Fransson, A., Chierici, M., Anderson, L.G., Bussman, I., Jones, E.P., Swift, J.H., 2001. The importance of shelf processes for the modification of chemical constituents in the waters of the eastern Arctic Ocean. Cont. Shelf Res. 21, 225–242.

Furevik, T., 2001. Annual and interannual variability of Atlantic water temperatures in the Norwegian and Barents Seas: 1980–1996. Deep-Sea Res., Part 1 48, 383–404.

Glover, D.M., Brewer, P.G., 1988. Estimates of wintertime mixed layer nutrient concentrations in the North Atlantic. Deep-Sea Res., Part 1 35, 1525–1546.

Gordeev, V.V., Martin, J.M., Sidorov, I.S., Sidorova, M.V., 1996. A reassessment of the Eurasian river input of water, sediment, major elements and nutrients to the Arctic Ocean. Am. J. Sci. 296 (6), 664–691.

Grasshof, K., 1983. Determination of nitrate. In: Grasshof, K., Ehrhardt, M., Kremling, K. (Eds.), Methods of Seawater Analysis, 2nd ed. Verlag Chemie, Weinheim, pp. 143–150.

Häkkinen, S., 2000. Simulated low-frequency modes of circulation in the Arctic Ocean. J. Geophys. Res. 105, 6549–6564.

Haraldsson, C., Anderson, L.G., Hassellöv, M., Hulth, S., Olsson, K., 1997. Rapid, high-precision potentiometric titration of alkalinity in the ocean and sediment pore waters. Deep-Sea Res., Part 1 44, 2031–2044.

Harris, C.L., Plueddemann, J., Gawarkiewicz, G.G., 1998. Water mass distributions and polar front structure in the western Barents Sea. J. Geophys. Res. 103, 2905–2917.

Holmen, K., 2001. Atmospheric carbon dioxide concentration at Ny-Ålesund (http://www.misu.su.se/~kim/pict/co2all.jpg).

Johnson, K.M., King, A.E., Sieburth, J.M., 1985. Coulometric TCO_2 analyses for marine studies: an introduction. Mar. Chem. 16, 61–82.

Johnson, K.M., Sieburth, J.M., Williams, P.J., Brandstrom, L., 1987. Coulometric total carbon dioxide analysis for marine studies: automation and calibration. Mar. Chem. 21, 117–133.

Körtzinger, A., Koeve, W., Kähler, P., Mintrop, L., 2001. C:N ratios in the mixed layer during the productive season in the northeast Atlantic Ocean. Deep-Sea Res., Part 1 48, 661–688.

Law, C., Martin, A.P., Liddicoat, M.I., Watson, A.J., Richards, K.J., Woodward, E.M.S., 2001. A Lagrangian SF_6 tracer study of an anticyclonic eddy in the North Atlantic: patch evolution, vertical mixing and nutrient supply to the mixed layer. Deep-Sea Res., Part 2 48, 705–724.

Lee, K., Millero, F.J., 1995. Thermodynamic studies of the carbonate system in seawater. Deep-Sea Res. 42, 2035–2061.

Lewis, E., Wallace, D.W.R., 1998. Program Developed for CO_2 System Calculations. ORNL/CDIAC-105. Carbon Dioxide Information Analysis Center, Oak Ridge National Laboratory, U.S. Department of Energy, Oak Ridge, TN.

Loeng, H., 1991. Features of the physical oceanographic conditions of the Barents Sea. Polar Res. 10 (1), 5–18.

Loeng, H., Ozhigin, V., Ådlandsvik, B., 1997. Water fluxes through the Barents Sea. ICES J. Mar. Sci. 54, 310–317.

Mauritzen, C., 1996. Production of dense overflow waters feeding the North Atlantic across the Greenland–Scotland ridge: 1. Evidence for a revised circulation scheme. Deep-Sea Res., Part 1 43, 769–806.

Michaels, A.F., Bates, N.R., Buesseler, K.O., Carlson, C.A., Knap, A.H., 1994. Carbon-cycle imbalances in the Sargasso Sea. Nature 372, 537–539.

Midttun, L., 1985. Formation of dense bottom water in the Barents Sea. Deep-Sea Res. 32, 1233–1241.

Midttun, L., 1989. Climatic fluctuations in the Barents Sea. Rapp. P.-V. Reun.-Cons. Int. Explor. Mer. 188, 23–35.

Olsson, K., Anderson, L.G., 1997. Input and biogeochemical transformation of dissolved carbon in the Siberian shelf seas. Cont. Shelf Res. 17, 819–833.

Redfield, A., Ketchum, B.H., Richards, F.A., 1963. The influence of organisms on the composition of sea water. In: Hill, M.N. (Ed.), The Sea, vol. 2. Wiley Interscience, New York, pp. 26–77.

Reigstad, M., Wassmann, P., Wexels Riser, C., Øygarden, S., Rey, F., 2002. Variation in hydrography, nutrients and chlorophyll *a* in the marginal ice zone and the central Barents Sea. J. Mar. Syst., this issue.

Roy, R.N., Roy, L.N., Vogel, K.M., Porter-Moore, C., Pearson, T., Good, C.E., Millero, F.J., Campbell, D.M., 1993. The dissociation constants of carbonic acid in seawater at salinities 5 to 45 and temperatures 0 to 45 °C. Mar. Chem. 44, 249–267.

Roy, R.N., Roy, L.N., Vogel, K.M., Porter-Moore, C., Pearson, T., Good, C.E., Millero, F.J., Campbell, D.M., 1994. Erratum for: The dissociation constants of carbonic acid in seawater at salinities 5 to 45 and temperatures 0 to 45 °C. Mar. Chem. 45, 337.

Sakshaug, E., Bjørge, A., Gulliksen, B., Loeng, H., Mehlum, F., 1994. Structure, biomass distribution, and energetics of the pelagic ecosystem in the Barents Sea: a synopsis. Polar Biol. 14, 405–411.

Sakshaug, E., Rey, F., Slagstad, D., 1995. Wind forcing of marine primary production in the northern atmospheric low-pressure belt. In: Skjoldal, H.R., Hopkins, C.E.C., Erikstad, K.E., Leinaas, H.P. (Eds.), Ecology of Fjords and Coastal Waters. Elsevier, Amsterdam, pp. 15–25.

Sambrotto, R.N., Savidge, G., Robinson, C., Boyd, P., Takahashi, T., Karl, D.M., Langdon, C., Chipman, D., Marra, J., Codispoti, L., 1993. Elevated consumption of carbon relative to nitrogen in the surface ocean. Nature 363, 248–250.

Schauer, U., Muench, R.D., Rudels, B., Timokhov, L., 1997. The impact of eastern Arctic shelf water on the Nansen Basin intermediate layers. J. Geophys. Res. 102, 3371–3382.

Schlosser, P., Bönisch, G., Kromer, B., Münnich, K.O., 1990. Ventilation rates in the Nansen Basin of the Arctic Ocean derived from a multitracer approach. J. Geophys. Res. 95, 3265–3272.

Skjoldal, R.H., Hassel, A., Rey, F., Loeng, H., 1987. Spring phytoplankton development and zooplankton reproduction in the central Barents Sea in the period 1979–1984. In: Loeng, H. (Ed.), Proceedings of the third Soviet–Norwegian Symposium, Murmansk, May 26–28, 1986. Institute of Marine Research, Bergen, pp. 59–89.

Slagstad, D., Wassmann, P., 1996. Climate change and carbon flux in the Barents Sea: 3-D simulations of ice-distribution, primary production and vertical export of particulate organic carbon. Polar Res. 51, 119–141, Special Issue.

Takahashi, T., Broecker, W.S., Langer, S., 1985. Redfield ratio based on chemical data from isopycnal surfaces. J. Geophys. Res. 90, 6907–6924.

Toggweiler, J.R., 1993. Oceanography—carbon overconsumption. Nature 363, 210–211.

Vinje, T., 1997. Ice fluxes through fram strait. Proceedings of the WCRP Conference on Polar Processes and Global Climate, ACSYS Project Office, November 3–6. Norwegian Polar Institute, Oslo.

Walsh, J.J., 1989. Arctic carbon sinks: present and future. Glob. Biogeochem. Cycles 3, 393–411.

Wanninkhof, R., 1992. Relationship between wind-speed and gas-exchange over the ocean. J. Geophys. Res. 97, 7373–7382.

Wassmann, P., Ratkova, T., Andreassen, I., Vernet, M., Pedersen, C., Rey, F., 1999. Spring bloom development in the marginal ice zone and the central Barents Sea. Mar. Ecol.-Pubbl. Stn. Zool. Napoli 20 (3–4), 321–346.